Progress In Electromagnetics Research C, Vol. 132, 117–127, 2023

Miniaturized Metamaterial Ultra-Wideband Antenna for WLAN and Bluetooth Applications

Gengliang Chen, Cong Guo, Jincheng Xue, Zhuopeng Wang, and Mingxiang Pang*

Abstract—In this paper, a new type of defected ground structure (DGS) antenna based on metamaterial is presented. The proposed antenna has the performance of global bandwidth and gain improvements. The miniaturization of the antenna can be achieved by loading metamaterials on the DGS antenna to reduce the resonance frequency of the antenna. Due to the coupling effect between the metamaterial and the DGS, multiple resonant points are generated, thus extending the impedance bandwidth of the antenna. The impedance bandwidth of the proposed antenna ranges from 3.5 GHz to 6.32 GHz (56.6%). The degree of miniaturization is 37.9%, and the measured peak gain is 4.5 dBi. The dimension of the antenna is only $0.35\lambda_0 \times 0.35\lambda_0 \times 0.011\lambda_0$, which has a highly stable antenna efficiency of greater than 90% over the entire operating bandwidth. The proposed antenna is suitable for WLAN and Bluetooth applications.

1. INTRODUCTION

With the technological progress in the field of communication and the rapid development of modern communication systems, the design requirements of antennas shift to the direction of miniaturization [1] and low cost. At present, when most antennas are miniaturized, the relative bandwidth is generally reduced, which greatly limits the practical application of antennas. Therefore, this paper aims to design a miniaturized ultra-wideband (UWB) antenna to solve the current situation of reducing relative bandwidth due to miniaturization.

Through the continuous development and utilization of the ground plane, current defected ground structure (DGS) is gradually formed. In [2–9], the performance of an antenna is improved by using different shapes of DGSs, so as to realize miniaturization. In [2], the DGS further improves the performance of the antenna by making a special notch treatment for a C-shaped slot. At the same time, a reflector plate is added to enhance the main lobe of the radiated signal, so as to improve the gain of the antenna. In [4], split ring resonators are placed on both sides of the feed line to improve the gain, and a DGS with stubs is placed to improve the bandwidth characteristics. At present, the large dimension of most antennas based on DGS design is not conducive to embedding objects or integration with other devices. However, the small dimension of a DGS requires greater accuracy for antenna fabrication due to maintaining precision.

Metamaterial has many different properties from other materials in nature. The combination design of metamaterial and antenna can change the performance of antenna. Due to its unique properties, metamaterials are widely used for antenna miniaturization, isolation enhancement, as well as changing polarization characteristics. In [10], a new type of metamaterial is designed. Three layers of metamaterial elements are placed along the ring to obtain a double-ring structure with ideal electromagnetic wave absorption characteristics. By loading the double-ring structure, the radar scattering cross section of the antenna is significantly reduced, and the radiation performance of the

Received 6 March 2023, Accepted 10 April 2023, Scheduled 19 April 2023
* Corresponding author: Mingxiang Pang (pangmingxiang@sdust.edu.cn).
The authors are with the College of Electronic and Information Engineering, Shandong University of Science and Technology, China.

antenna is not degraded. In [11–13], metasurface elements of different shapes are periodically arranged to improve the impedance bandwidth and gain of the antenna. In [14], the reactive impedance surface and complementary resonant ring are loaded, and the design is very complex due to the multilayer structure of the antenna. In [15, 16], the antenna miniaturization of a circular patch and slot antenna is realized due to the resistive load effect.

In this paper, a simple-shape metamaterial is designed first, and then a new metamaterial structure is formed by combining heterogeneous metamaterial. Metamaterials are loaded on the basis of a DGS antenna, making full use of the defective ground structure and gradually reducing the resonance point of the antenna to achieve the required frequency band. The proposed antenna contains multiple useful wireless frequency bands, which extend the bandwidth based on the miniaturization of the antenna. It solves the problem of narrow bandwidth caused by smaller antenna dimension in many current papers. The proposed antenna is suitable for WLAN and Bluetooth applications.

2. METAMATERIAL DESIGN

In this paper, we first propose a metamaterial structure with heterogeneous open ring (HOR), which is named metamaterial I. It consists of two nested open rings (ORs) printed on the same surface of the dielectric substrate. An HOR is composed of a arc arm and two straight arms, printed on an epoxy resin (FR4) dielectric substrate. The structure of metamaterial I is shown in Figure 1. When the electromagnetic wave is incident vertically, the reflection coefficient is shown in Figure 2. It can be seen that the reflection coefficient of the metamaterial has a minimum value at 3.2 GHz, while the phase changes drastically at this frequency.

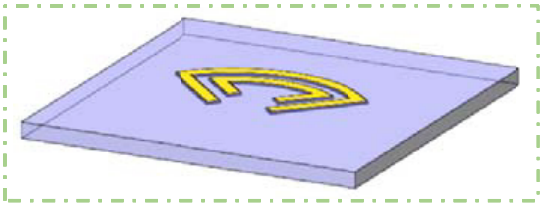

Figure 1. The structure of metamaterial I.

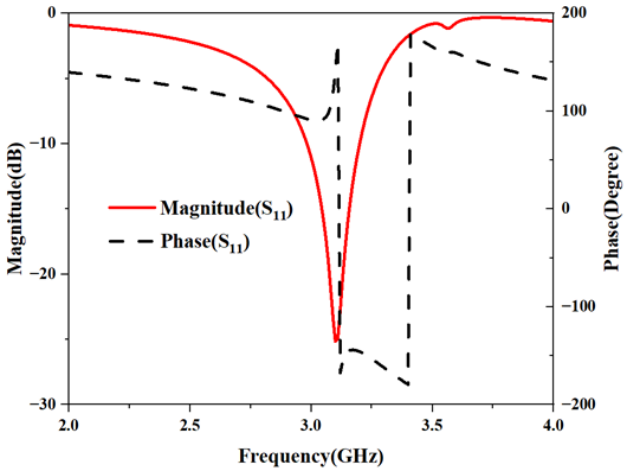

Figure 2. Amplitude and phase of reflection coefficient of metamaterial.

An equivalent circuit model was used to analyze the HOR metamaterial structure. Inductive current will be formed on the OR, and the structure will introduce inductors. The gap between the ORs forms the two plates of the capacitance, so capacitors will be introduced. Although the equivalent circuit model of metamaterials can be obtained by theoretical method, the difficulty of this method is the calculation of the specific value of each electronic component in the equivalent circuit. Therefore, we simulated and optimized the equivalent circuit through Advanced Design System (ADS). Figure 3 shows the equivalent circuit model obtained by ADS simulation of this structure, where $L_1 = 1.5\,\text{nH}$, $L_2 = 2.5\,\text{nH}$, $L_3 = 0.7\,\text{nH}$, $L_4 = 0.5\,\text{nH}$, $C_1 = 1\,\text{pF}$, $C_2 = 0.5\,\text{pF}$, $C_3 = 0.2\,\text{pF}$, $C_4 = 0.2\,\text{pF}$, and $C_5 = 1.7\,\text{pF}$. L_1, L_2, L_3, and L_4 are loop inductors; C_1, C_2, and C_4 are coupling capacitors generated by the inner open rings and outer open rings; and C_3 and C_5 are resonant capacitors generated by the open rings. Figure 4 shows the simulation results of the equivalent circuit in ADS. It can be seen that the phase of the equivalent circuit model changes sharply at 3.2 GHz, which is consistent with the

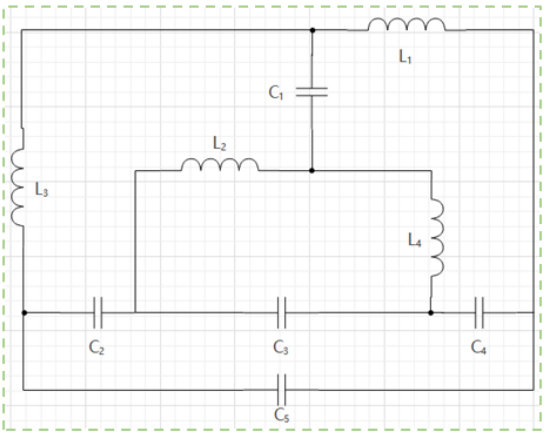

Figure 3. Equivalent circuit model of HOR.

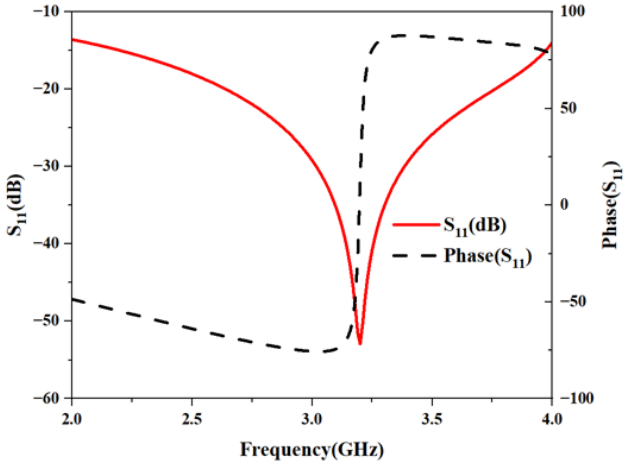

Figure 4. Simulation results of equivalent circuit model in ADS.

electromagnetic simulation results of metamaterials. Therefore, we believe that the equivalent circuit model we designed is correct.

This HOR metamaterial is different from conventional OR. It increases the capacitance and inductance of the circuit through the nesting of two open rings, thereby reducing the resonant frequency of the loop. Next, the equivalent permittivity and permeability of the metamaterial model are calculated.

Firstly, complex S parameters [21] of metamaterials can be obtained by electromagnetic simulation:

$$S_{11} = \frac{R(1-T^2)}{1-R^2T^2} \tag{1}$$

$$S_{21} = \frac{T(1-R^2)}{1-R^2T^2} \tag{2}$$

R and T are respectively:

$$R = \frac{2S_{11}}{1+S_{11}^2-S_{21}^2 \pm S} \tag{3}$$

$$T = \frac{1-S_{11}^2+S_{21}^2 \pm S}{2S_{21}} \tag{4}$$

In formula:

$$S = \sqrt{1-2S_{11}^2-2S_{21}^2-2S_{11}^2S_{21}^2+S_{11}^4+S_{21}^4} \tag{5}$$

The equivalent permittivity and equivalent permeability of the equivalent homogeneous medium can be approximated by the following formula:

$$\varepsilon \approx \frac{2}{jkd}\frac{1-v_1}{1+v_1} \tag{6}$$

$$\mu \approx \frac{2}{jkd}\frac{1-v_2}{1+v_2} \tag{7}$$

where $v_1 = S_{21}+S_{11}$, $v_2 = S_{21}-S_{11}$, $k = \omega/c$, d is the thickness of the medium.

The equivalent permittivity and permeability of the HOR metamaterial are calculated using the formula, and the results are shown in Figure 5. It can be seen that the real part of the permittivity has negative values within 3.3 GHz–6.0 GHz, 6.2 GHz–7.0 GHz. In the 3.0 GHz–5.5 GHz band, the real part of the permeability has negative values. The OR can be regarded as a magnetic resonance, where an inductive current is generated in the OR when an electromagnetic wave is incident, thereby introducing inductors. Two ORs form an electrical resonance, and the open rings are coupled to each other, thus introducing coupling capacitors. Therefore, it can be concluded that the electrical resonance and

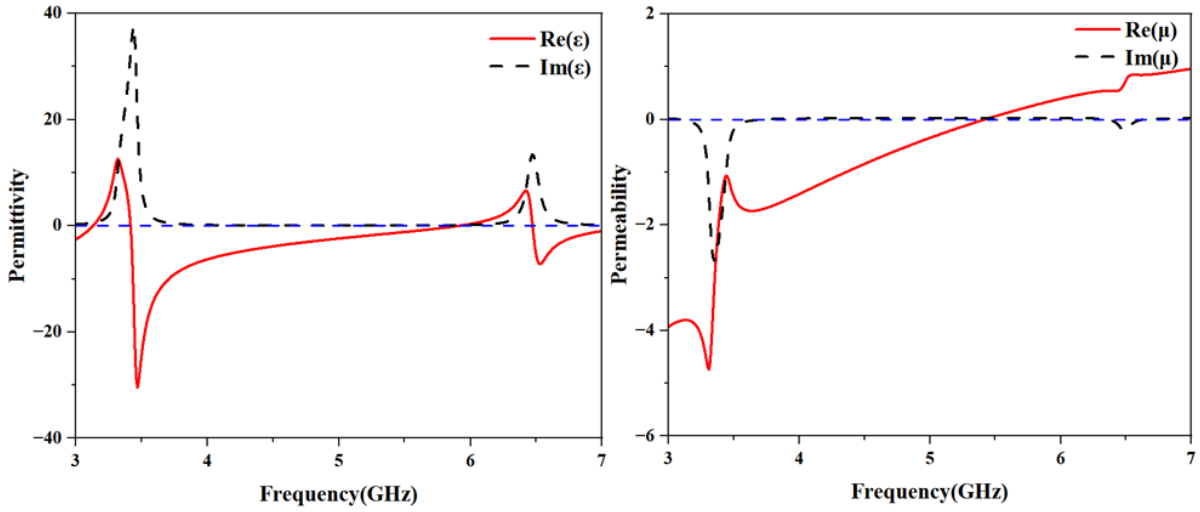

Figure 5. Equivalent permittivity and equivalent permeability of the metamaterial I.

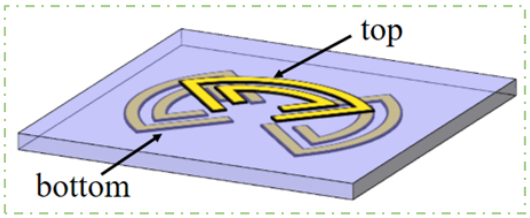

Figure 6. The structure of metamaterial II.

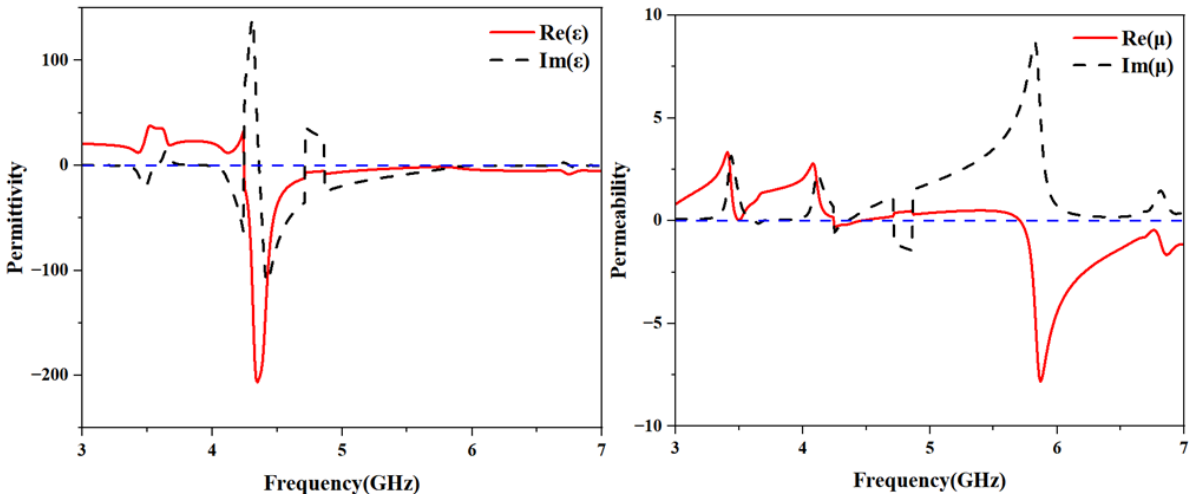

Figure 7. Equivalent permittivity and equivalent permeability of the metamaterial II.

magnetic resonance of the HOR occur at the above frequency bands, resulting in the metamaterial characteristics of negative permittivity and negative permeability.

On the basis of metamaterial I, two rotational symmetric HOR metamaterial structures are loaded on the bottom of the substrate to form a new metamaterial structure II. The structure of metamaterial II is shown in Figure 6. The equivalent permittivity and permeability of the metamaterial II are shown in Figure 7. It can be seen that in the 4.2 GHz–7.0 GHz frequency band, the real part of the permittivity

has negative values. In the 4.2 GHz–4.5 GHz and 5.7 GHz–7.0 GHz bands, the permeability has negative values. Because the coupling between the elements of metamaterial and will have influence on the field distribution, the equivalent electromagnetic parameters of metamaterial II are different from that of metamaterial I. It can be concluded that the three HOR structures form a novel metamaterial structure with metamaterial properties of negative permittivity and negative permeability.

3. ANTENNA STRUCTURE AND DESIGN PROCESS

In this paper, a miniaturized metamaterial UWB antenna based on a defective ground structure [3] is proposed. The working principle of the DGS is to disturb the current distribution on the ground by etching different shapes of patterns on the metal floor, so as to change the transmission characteristics parameters of the microwave circuit. The antenna is fed by a rectangular microstrip line and supported by a circular defect ground structure etched on the ground surface. The metamaterials are loaded on the defect ground antenna. The antenna is printed on an FR4 substrate. Figure 8 shows the antenna structure diagram designed in this paper. The optimized antenna design parameters are shown in Table 1.

$$L_1 = 0.083 \cdot \frac{c}{f_0\sqrt{\varepsilon_r}} \tag{8}$$

$$L_2 = \frac{c}{2f_0\sqrt{\varepsilon_r}} \tag{9}$$

Formula (8) is the relationship between the width of the feed line and the resonant frequency of the DGS antenna; formula (9) is the relationship between the length of the feed line and the resonant frequency

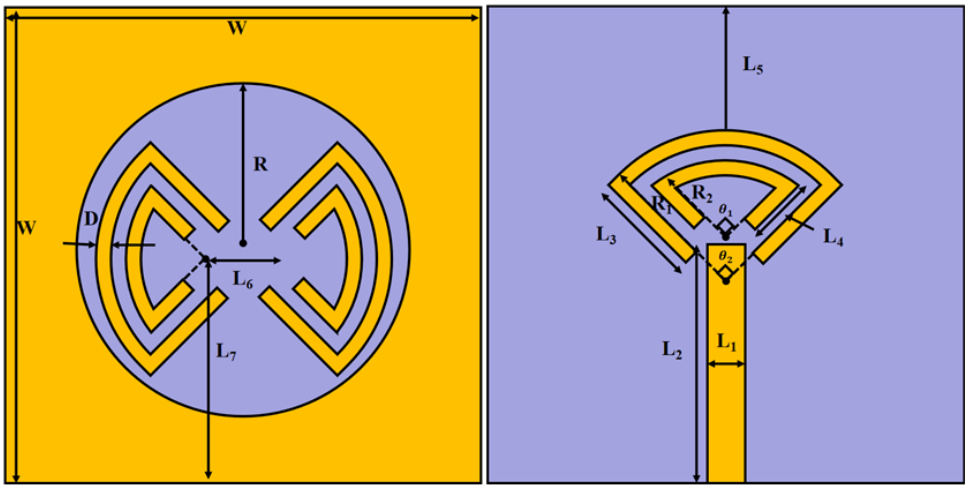

Figure 8. Antenna structure. (a) Top view. (b) Bottom view.

Table 1. The dimension of the proposed antenna.

Parameter	W	R	R_1	R_2	D	L_1
Dimension (mm)	30	10	10	8	1	2
Parameter	L_2	L_3	L_4	L_5	L_6	L_7
Dimension (mm)	13	6	3	10	4	14.7
Parameter	θ_1	θ_2				
Dimension (°)	90	90				

of the DGS antenna [3]; c is the speed of light in vacuum, and its unit is m/s; f_0 is the resonant frequency of the defective ground antenna, and its unit is GHz; ε_r is the effective dielectric constant of the substrate.

$$\rho = \frac{f_2 - f_1}{f_2} \times 100\% \tag{10}$$

Formula (10) represents the miniaturization degree of the antenna; f_2 is the resonant frequency of the antenna without the metamaterial; and f_1 is the resonant frequency of the antenna after loading the metamaterial.

The design process of DGS antenna loaded with HOR is shown in Figure 9. The initial design was a common DGS antenna with a resonant frequency at 5.6 GHz. On the basis of antenna A, metamaterial I is placed on the top of the rectangular microstrip feed line to form electrical resonance, so as to realize antenna B. It can be seen from Figure 10 that the resonant frequency of the antenna is reduced from 5.6 GHz to 4.6 GHz, and the miniaturization degree reaches 17.8%. In order to further realize the miniaturization of the antenna, two HORs are placed in the defect ground to form metamaterial II; then

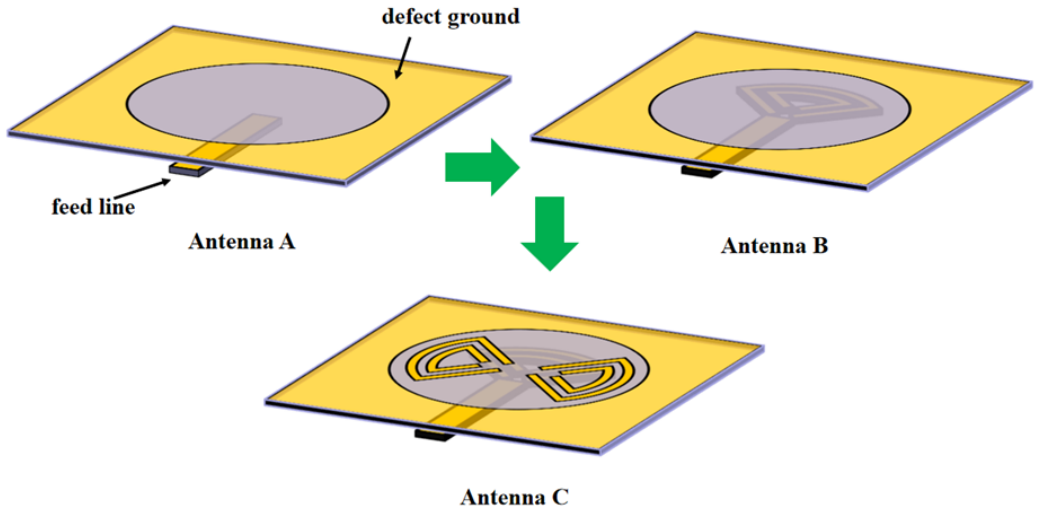

Figure 9. The design procedure of the proposed antenna.

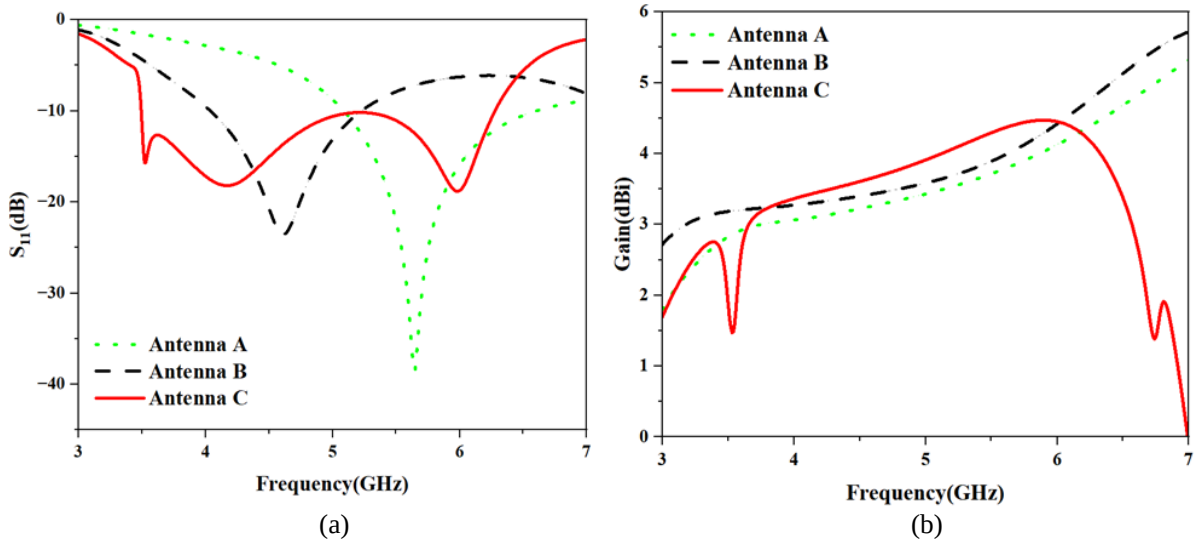

Figure 10. Simulation of three antenna designs. (a) S_{11}. (b) Gain.

another HOR is placed; finally antenna C is realized based on antenna B. The metamaterials are loaded into the DGS antenna, and multiple resonant points are formed through excitation coupling to broaden the bandwidth. Further, the resonant frequency of the antenna is reduced from 4.6 GHz to 3.5 GHz, and the gain in the working band is improved to some extent, with the degree of miniaturization reaching 37.9% and the relative bandwidth reaching 56.6%.

4. PARAMETRIC STUDY

Figure 11 shows the simulation of S_{11} with different positions of HOR at the top of the feed line. As shown in Figure 11, when L_5 varies between 8.0 mm and 11.0 mm, the resonance point and the operating bandwidth will change. The equivalent electromagnetic parameters of metamaterial II vary with the variation of L_5. The field distribution of the antenna changes accordingly, which ultimately affects the performance of the antenna. According to the simulated S_{11} obtained by different L_5 values, the position of the HOR is selected as $L_5 = 10.0$ mm.

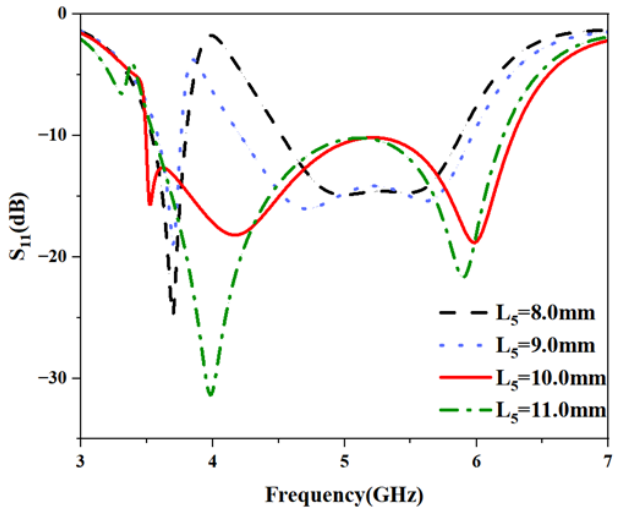

Figure 11. Simulated S_{11} for various values of L_5.

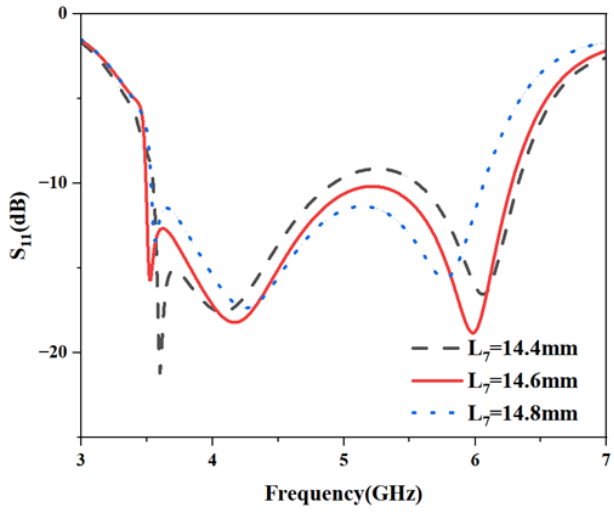

Figure 12. Simulated S_{11} for various values of L_7.

Figure 12 shows the simulated S_{11} of the HOR that are located differently in the defect ground. As shown in Figure 12, when L_7 varies between 14.4 mm and 14.8 mm, the operating bandwidth of the defective antenna will change. The equivalent electromagnetic parameters of metamaterial II vary with the variation of L_7, which ultimately affects the performance of the antenna. When $L_7 = 14.6$ mm or 14.8 mm, the minimum resonance point of the antenna is located at 3.5 GHz. However, when $L_7 = 14.6$ mm, the operating bandwidth of the antenna is wider.

5. SIMULATED AND MEASURED RESULTS

Simulation results of S_{11}, current, and gain are obtained by electromagnetic simulation software HFSS. The proposed metamaterial antenna is manufactured and measured, and the simulation results are verified. In Figure 13, the measured impedance bandwidth of the antenna is 3.6 GHz–6.42 GHz, meeting the design requirements of ultra-wideband, and the simulation gain of the antenna is in good consistency with the measurement gain. Due to the errors in the fabrication and measurement of the antenna, there is a slight error between the simulated S_{11} and measured S_{11}, but this error is within expected fabrication tolerances. Figure 14 shows the radiation pattern of the metamaterial antenna at 4.5 GHz and 6.0 GHz, and it can be observed that the antenna maintains omnidirectional characteristics. We compare the antenna designed in this paper with other miniaturized antennas. It can be seen that the

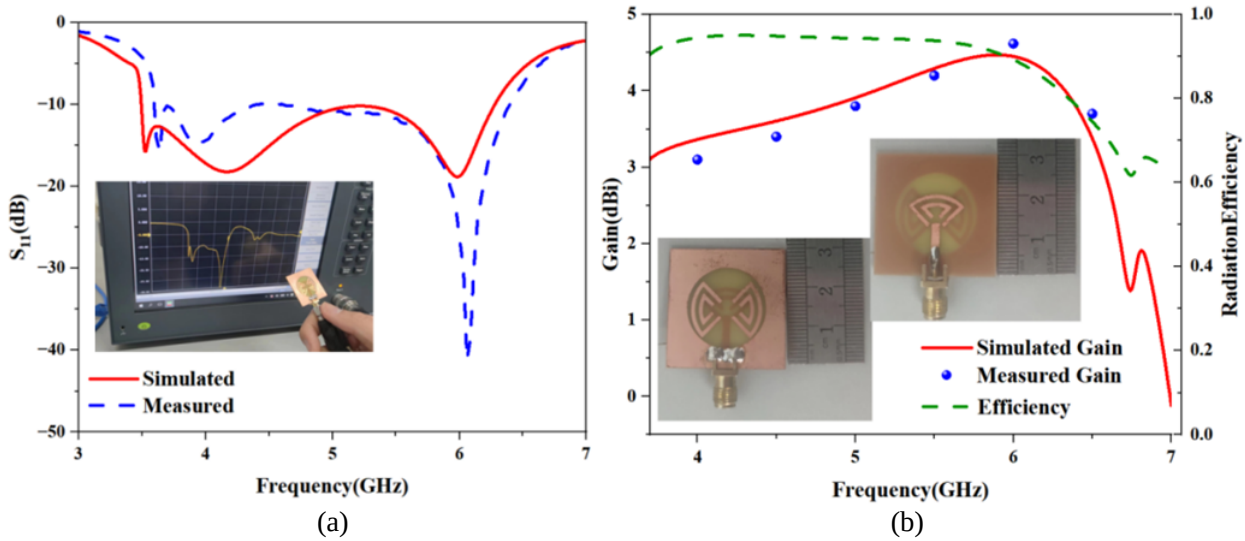

Figure 13. Simulated and measured results. (a) S_{11}. (b) Gain, efficiency.

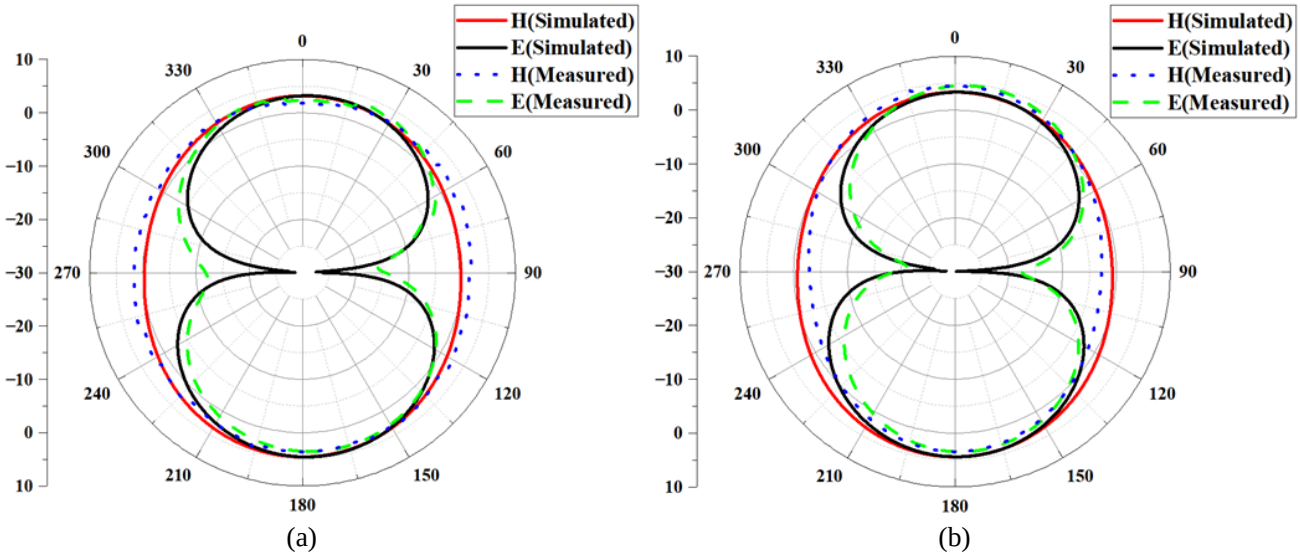

Figure 14. Simulated and measured results of radiation pattern. (a) 4.5 GHz, (b) 6.0 GHz.

Table 2. Proposed antenna comparison with previous.

Reference	Overall dimension	Resonance (GHz)	Miniaturization (%)	−10 dB Bandwidth (%)
[17]	$0.39\lambda_0 \times 0.36\lambda_0 \times 0.042\lambda_0$	2.55	33%	1.2%
[18]	$0.47\lambda_0 \times 0.47\lambda_0 \times 0.024\lambda_0$	3.51	30%	2.3%
[19]	$0.20\lambda_0 \times 0.12\lambda_0 \times 0.029\lambda_0$	2.57	36.4%	26.4%
[20]	$0.34\lambda_0 \times 0.34\lambda_0 \times 0.013\lambda_0$	3.4	45%	3.8%
Proposed antenna	$0.35\lambda_0 \times 0.35\lambda_0 \times 0.011\lambda_0$	3.53	37.9%	56.6%

antenna designed in this paper not only achieves miniaturization, but also greatly improves the relative impedance bandwidth of the antenna. Table 2 compares the performance of the antenna designed in this paper with other papers.

Figure 15 shows that when the antenna operates at 4.2 GHz, the current is mainly concentrated on the feed line and metamaterial I. It can be concluded that the miniaturization of the antenna is achieved when the metamaterial I works. When the antenna works at 3.5 GHz, the current mainly concentrates on the feed line and metamaterial II. It can be seen that the work of metamaterial II is the main factor to further realize the miniaturization of the antenna.

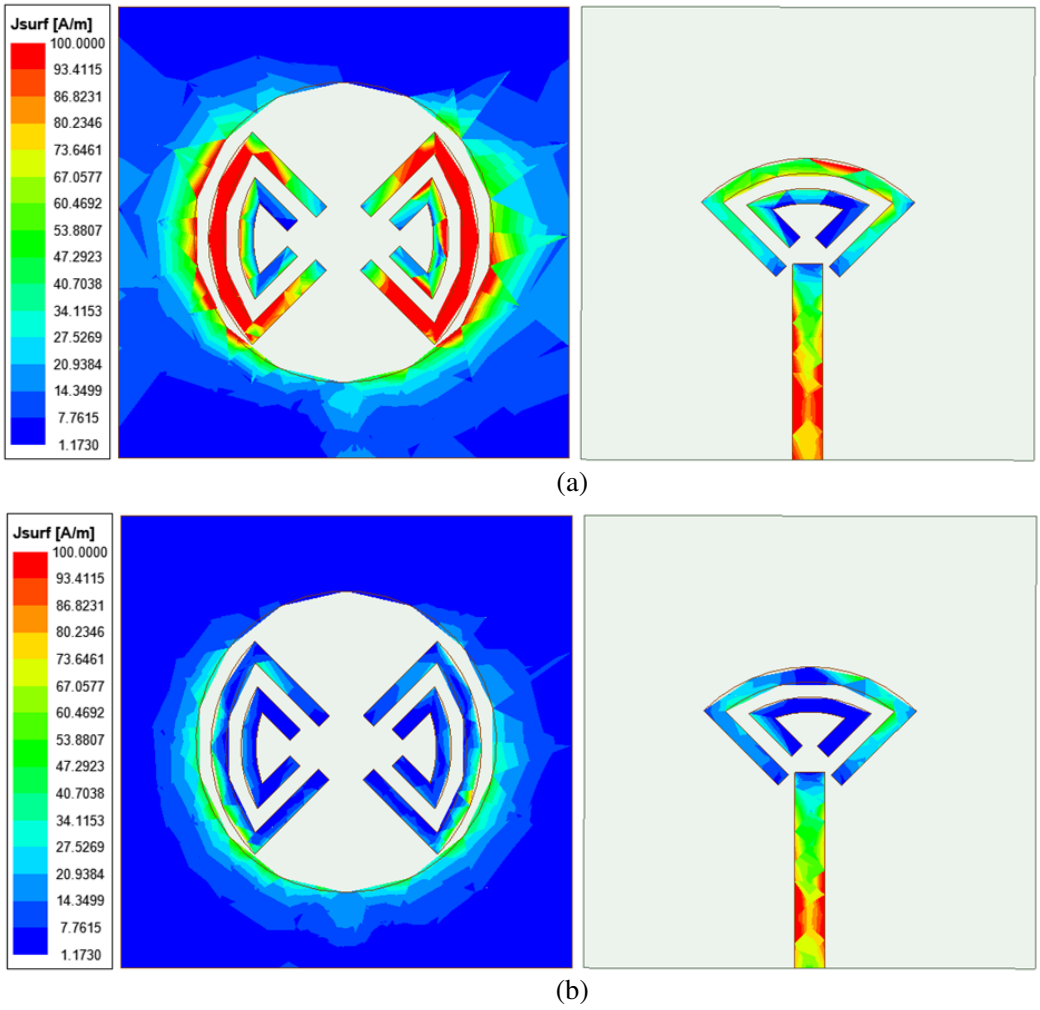

Figure 15. Current distribution diagram of antenna surface. (a) 3.5 GHz, (b) 4.2 GHz.

6. CONCLUSION

In this paper, a novel HOR metamaterial is proposed, and the metamaterial is gradually loaded into the defective ground antenna to achieve two left shifts of the resonant frequency. The measured results show that the metamaterials designed in this paper can reduce the dimension of the antenna, broaden the impedance bandwidth of the antenna, and achieve a slight improvement of the gain. This method using HOR metamaterials to reduce antenna dimension without damaging the relative bandwidth provides a new idea and method for antenna miniaturization, which is helpful for promoting the practical application of metamaterials.

REFERENCES

1. Salih, A. A. and M. S. Sharawi, "A dual-band highly miniaturized patch antenna," *IEEE Antennas and Wireless Propagation Letters*, Vol. 15, 1783–1786, 2016.
2. Olawoye, T. O. and P. Kumar, "A high gain microstrip patch antenna with slotted ground plane for sub-6 GHz 5G communications," *2020 International Conference on Artificial Intelligence, Big Data, Computing, and Data Communication Systems (icABCD)*, 2020.
3. Asghar, M., S. Lupin, S. Shoaib, and P. Excell, "Design and analysis of compact antenna for 5G communication devices," *2020 IEEE Conference of Russian Young Researchers in Electrical and Electronic Engineering (EIConRus)*, 2020.
4. Patchala, K., Y. R. Rao, and A. M. Prasad, "Triple band notch compact MIMO antenna with defected ground structure and split ring resonator for wideband applications," *Heliyon*, Vol. 6, e03078, 2020.
5. Nor, M. Z. M., S. K. A. Rahim, M. I. Sabran, et al., "Slotted dual band directive antenna with defected ground plane structure," *Microwave Conference Proceedings*, 432–434, IEEE, 2014.
6. Yadav, N. P., "Triple U slot loaded defected ground plane antenna for multiband operations," *Microwave and Optical Technology Letters*, Vol. 58, No. 1, 124–128, 2016.
7. Pei, J., A. G. Wang, S. Gao, et al., "Miniaturized triple-band antenna with a defected ground plane for WLAN/WiMAX applications," *IEEE Antennas and Wireless Propagation Letters*, Vol. 10, No. 4, 298–301, 2011.
8. Thomas, K. G. and M. Sreenivasan, "Compact triple band antenna for WLAN/WiMAX applications," *Electronics Letters*, Vol. 45, No. 16, 811–813, 2009.
9. Sarkar, S., A. D. Majumdar, S. Mondal, et al., "Miniaturization of rectangular microstrip patch antenna using optimized single-slotted ground plane," *Microwave and Optical Technology Letters*, Vol. 53, No. 1, 111–115, 2015.
10. Ren, J., S. Gong, and W. Jiang, "Low-RCS monopolar patch antenna based on a dual-ring metamaterial absorber," *IEEE Antennas and Wireless Propagation Letters*, Vol. 17, No. 1, 102–105, Jan. 2018, doi: 10.1109/LAWP.2017.2776978.
11. Kedze, K. E., H. Wang, and I. Park, "A metasurface-based wide-bandwidth and high-gain circularly polarized patch antenna," *IEEE Transactions on Antennas and Propagation*, Vol. 70, No. 1, Jan. 2022.
12. Xue, M., W. Wan, Q. Wang, and L. Cao, "Low-profile millimeter-wave broadband metasurface antenna with four resonances," *IEEE Antennas and Wireless Propagation Letters*, Vol. 20, No. 4, Apr. 2021.
13. Hossain, B. and F. Hossain, "A dual band microstrip patch antenna with metamaterial superstrate for biomedical applications," *2021 International Conference on Electronics, Communications and Information Technology (ICECIT)*, Sep. 14–16, 2021.
14. Dong, Y., H. Toyao, and T. Itoh, "Design and characterization of miniaturized patch antennas loaded with complementary split-ring resonators," *IEEE Transactions on Antennas and Propagation*, Vol. 60, No. 2, 772–785, Feb. 2012. email
15. Ouedraogo, R. O., E. J. Rothwell, A. R. Diaz, K. Fuchi, and A. Temme, "Miniaturization of patch antennas using a metamaterial-inspired technique," *IEEE Transactions on Antennas and Propagation*, Vol. 60, No. 5, 2175–2182, May 2012.
16. T. Shaw, D. Bhattacharjee, and D. Mitra, "Miniaturization of slot antenna using split ring resonators," *IEEE AEMC*, Guwahati, India, Dec. 2015.
17. Zhang, B. and X. Xu, "Design of a miniaturized annular ring metamaterial microstrip antenna," *2021 International Symposium on Antennas and Propagation (ISAP)*, 1–2, Taipei, Taiwan, 2021.
18. Dai, G., X. Xu, and X. Deng, "Miniaturized semicircular disc patch antenna designed with sector-shaped metamaterials," *2020 International Symposium on Antennas and Propagation (ISAP)*, 409–410, Osaka, Japan, 2021.

19. Saghanezhad, S. A. H. and Z. Atlasbaf, "Miniaturized dual-band CPW-fed antennas loaded with U-shaped metamaterials," *IEEE Antennas and Wireless Propagation Letters*, Vol. 14, 658–661, 2015.
20. Shaw, T. and G. Samanta, "Miniaturized slot antenna design using high permittivity & permeability property of metamaterial," *2021 IEEE Indian Conference on Antennas and Propagation (InCAP)*, 1–4, Jaipur, Rajasthan, India, 2021.
21. Smith, D. R., D. C. Vier, and T. Koschny, "Electromagnetic parameter retrieval from inhomogeneous metamaterials," *Physical Review E. Statistical, Nonlinear, and Soft Matter Physics*, Vol. 71, 036617, 2005.